scientific reports

Check for updates

OPEN

Investigating antibacterial activity of biosynthesized silver oxide nanoparticles using *Phragmanthera Macrosolen L*. leaf extract

Abel Saka[1,2], Suhash Ranjan Dey[1], Leta Tesfaye Jule[2], Ramaswamy Krishnaraj[3,4,6]✉, Rengasamy Dhanabal[1], Neha Mishra[1] & N. Nagaprasad[5]

The crude leaf extract of *Phragmanthera macrosolen L*. has been utilized for the first time as an effective reducing, capping and stabilizing agent to synthesize silver oxide nanoparticles (Ag_2O NPs) through a green approach. The prepared Ag_2O NPs were analyzed by scanning electron-microscopy (SEM), High Resolution Transmission electron microscope (HR-TEM), X-ray diffractions (XRD), Fourier transforms infrared (FTIR) spectroscopy, energy dispersive spectroscopy (EDS), and Ultra-violet visible spectrometry (UV-Vis). The biosynthesized Ag_2O NPs applied on gram-positive (*S. aureus*) and gram-negative (*E. coli*) bacterial types. FTIR spectral peaks indicate that the phytochemicals in the extract are responsible for the formation of Ag_2O nanoparticles. The XRD result shown, poly-crystalline nanoparticles and the average crystalline size calculated was 45.8 nm. UV-Vis analysis shows absorbance existed at 590.5 nm, and the energy band gap calculated through the Tauc relation was 2.1 eV. The SEM images gave a globular and some rod like morphology with diameter of particle obtained between 20.11 and 46.50 nm with some hollow cubic microstructure of Ag_2O NPs which makes it suitable for antimicrobial application. The EDS confirms the elemental composition and existence of Ag and O_2. The HR-TEM images, specific area electron diffraction (SAED), and XRD patterns confirmed the morphology of Ag_2O NPs mean 45.84 nm and polycrystalline nature of the nanoparticles. The minimum inhibitory concentration (MIC) and minimum bactericidal concentration (MBC) were 15 and 30 µl respectively for the samples tested. In this study, it was observed that Ag_2O NPs highly sensitive to *E. coli* than *s. aureus*. The present study revealed that the possible use of green synthesized Ag_2O NPs as potential antibacterial agent.

Keywords Antibacterial, Characterization, Green synthesis, Leaf extract, Silver oxide

Nanotechnology is one that is categorized under upcoming fields of study in the recent research area of condensed matter sciences. It shows absolutely novel characteristics, like sizes, structures and morphologies of the particles[1]. Metallic oxide nanomaterials have gained specific attentions due to their unique physicochemical properties with great potentials in environment remediation[2,3]. Their use ranges from the removal of heavyweight metals, toxic gas-sensing, fabrics, bio-medical application, and photo-catalytic degradations of organic contaminant[4,5]. Ag_2O NPs were newly initiated to have special characteristics for application in solar cells, sensor, storage device, medical applications, as well as photo-catalysis[6,7]. Ag_2O NPs have been discovered in several investigational studies concentrating on their preparation, analysis techniques, and photo-catalytic performances. Their virtuous optical characteristics as well as narrow energy band gap (1.2-2.4 eV), which permits them to absorb the photovoltaic spectrums. Ag_2O NPs photo-catalyst was also published to experience self-stabilizing procedure during photo-catalytic degradations of organic compound, ensuing in a great photo-catalytic performance[8].

[1]Combinatorial Materials Laboratory, Department of Materials Science and Metallurgical Engineering, Indian Institute of Technology, Hyderabad 502284, India. [2]Department of Physics, College of Natural and Computational Science, Dambi Dollo University, Dambi Dollo, Ethiopia. [3]Department of Mechanical Engineering, Dambi Dollo University, Dambi Dollo, Ethiopia. [4]Centre for Excellence-Indigenous Knowledge, Innovative Technology Transfer, and Entrepreneurship, Dambi Dollo University, Dambi Dollo, Ethiopia. [5]Department of Mechanical Engineering, ULTRA College of Engineering and Technology, Madurai 625 104, Tamil Nadu, India. [6]Center for Global Health Research, Saveetha Institute of Medical and Technical Sciences, Saveetha University, Chennai, India. ✉email: prof.dr.krishnaraj@dadu.edu.et

Synthesis methods of Ag_2O NPs, is one of the further encouraging area of nano technology[9]. Ag_2O NPs have been prepared by through several physical and chemical methods such as chemical reductions[10,11], laser ablation[12,13], microwave irradiation[14] and solvo-thermal. Though chemical as well as physical approaches may efficiently produce pure nanomaterials, but these techniques are quite costly and potentially dangerous to the atmosphere. Chemical root for nanoparticle preparation uses poison chemicals, whereas physical root releases poisonous byproducts, harmful to the environments. In the combustions root, citric-acid, urea, and glycine- are utilized as fuels through nanoparticles synthesis. In current times, the combustions root categorized as solutions combustions synthesis, Conventionally (SHS): condensed phases combustions, and sol gel based combustions[15,16]. The foremost challenge of this technique is uncontrollability on phases as well as surface morphologies, but in current few years, certain advancement in phases and surface morphologies control has been perceived[17]. Therefore there is appropriate need to use a green synthesis method which is ecologically gentle, eco-friendly methods for nanoparticles fabrications extracting plant's parts. The basic principles of green root for the fabrications of metallic oxide nanoparticles are reductions of metal complexes in the weak solutions to get metallic colloids dispersion. Hydrazine's hydrate and sodium borohydride are commonly acknowledged reducing agents, however they are favored due to their toxic soak them through the prepared nanoparticles[18].

Rare reported regarding the green synthesis of Ag_2O NPs through plant leaf extracts. To mention some of them are *Lippia-citriodora*[19], *Ficus-benghalensis*[20], *Telfairia occidentalis*[21], *Azadirachta-indica*[22], *Artemisia Herba-Alba*[23], *Centella Asiatica*[24], *Mentha-pulegium* and *Ficus carica*[25], *Zephyranthes Rosea*[26], *Rhamnus virgata*[27], Curcuma zanthorrhiza[28], *Panicum miliaceum*[29], *Cyathea nilgiriensis Holttum*[30], and *Bacillus paramycoides*[31]. The researchers have been paying attention to green-chemistry to increase and protection of environment. The applications of silver oxide nanoparticles are wide, starting from photo-catalysis[32], medicinal value, and drug delivery[33]. Pharmaceutically, Ag_2O nanoparticles have been used for treating diseases like malaria, cancer treatment, tuberculosis and diabetes[30,34–36]. Additionally, silver-based nano particles are extensively applied for their exclusive characteristics in chemical identifying, bio-sensing, photonic activities and opto-electronics[37]. They have an excessive potential in medical applications like anti-microbial activities[38].

Green chemistry grounded approaches have been stated in the preparation of nano particles in current years, amongst the numerous chemical and physical methods of nano particle production[39]. Plant body extracts have been applied to serve as reducing, capping, and stabilizing agents in the preparation of nanoparticles. These extracts do not contain any laboratory-prepared chemical mixtures on their surfaces, making them non-toxic to humans and the environment[40,41]. Ag_2O is an excellent semi-conducting material, widely used in sensors, solar cells, fuel cells, and corrosion catalysis[42]. The exceeding reports provide information roughly the significances of the Ag_2O NPs as well as its performance researches on biosynthesis for bio-medical and agricultural solicitations. However green synthesis of Ag_2O NPs from traditional medicinal plants were rarely reported. In our knowledge there is no report on synthesis of Ag_2O NPs using the novel *Phragmanthera macrosolen* leaf extract; without using any other chemical reagents as reducing agent. Current work displays green preparation of Ag_2O NPs using *Phragmanthera macrosolen* leaf extracts, characterizations and antibacterial activities. Mistletoe, a common name used generally for woody shoot parasites, belongs to the order Santalales, it includes *Loranthaceae*, *Santalaceae*, and *Misodendraceae* families[43]. The novel plant mistletoe of Albizia *Gummifera*, which is known as *Phragmanthera macrosolen* from *Loranthaceae* family selected for this work due to its availability and traditionally usable for different medical values in the research location conducted. In this study, Ag_2O NPs were synthesized by novel approach using *Phragmanthera macrosolen* and its antibacterial activity against gram negative bacteria (*E. coli*) and gram-positive bacteria (*S. aureus*) were investigated.

Materials and methods

Materials

Silver-nitrate ($AgNO_3$)-99% was bought from Sigma Aldrich company, through Indian Institute of Technology, Hyderabad. All chemicals as well as substances utilized were of extremely pure analytical grades. A leaf of mistletoes of Albizia Gummifera (*Phragmanthera macrosolen L.*) was gathered from Dambi Dollo University, and Dambi Dollo Town, Oromia, Ethiopia. The plant we have used in this report was cultivated in Dambi Dollo University research center, Oromia, Ethiopia. This study complies with relevant international, national, institutional and legislative guidelines.

Phyto-chemical screening

Phyto-chemical screening with chemicals to test the content of bioactive compounds in 80% ethanol extracts of *Phragmanthera macrosolen L.* leaf. The Phyto-chemical test contains the bioactive compounds by reagents tests of 80% ethanol rigorous extracts from *Phragmanthera macrosolen L.* leaf plants. The bioactive compounds were tested following previously reported methods with changing the leaves with *Phragmanthera macrosolen L*[44–48].

Flavonoid tests

Leaf extracts of *Phragmanthera macrosolen L.* with a concentration of 1000 mg/L were transferred into test tubes in a volume of 0.5mL. Subsequently, they were liquefied in 2 mL of hot 50% methanol solvent. Following this, the mixture was combined with magnesium metal and a few drops of concentrated hydrochloric acid. The automatically observed orange-colored solution indicated the presence of flavonoids in the *Phragmanthera macrosolen L.* leaf.

Alkaloid tests

Leaf extracts of *Phragmanthera macrosolen L.* with a concentration of 1000 mg/L were dispensed into test tubes at a volume of 0.5 mL. Subsequently, 0.5 mL of 2% hydrochloric acid was added to the solutions, and the resulting mixtures were divided among three test tubes. Test tube 1 received an additional 0.5 mL of dilute acid solution

for comparison, test tube 2 was supplemented with 2–3 drops of Dragendorff reagent, and test tube 3 was treated with 2–3 drops of Mayer reagent. A positive indication for alkaloids was confirmed if an orange precipitate formed in test tube 2 and a yellowish-white deposit formed in test tube 3.

Sesquiterpenoid tests
Leaf extracts of *Phragmanthera macrosolen L*. with a concentration of 1000 mg/L were introduced into the test tube at a volume of 0.5 mL. Subsequently, diethyl ether was added, and the mixture was shaken. The ether layer was then separated and evaporated using a vaporizer cup positioned above a water bath. The resulting filtrate was combined with 10% vanillin in H_2SO_4. The absence of a color change in the solution indicated the non-existence of Sesquiterpenoid in the *Phragmanthera macrosolen L*. leaf.

Carbohydrates tests
In the Fehling's test, 5 mL of Fehling's solution was introduced to 0.5 mg of *Phragmanthera macrosolen L*. extract, followed by boiling in a water bath. The emergence of a yellow or red precipitate signals the existence of reducing power. For the Benedict's test, 5 mL of Benedict's solution was applied to 0.5 mg of the extract and subjected to boiling in a water bath. The formation of a yellow precipitate indicates the presence of reducing sugars.

Phlobatannins tests
The lack of a red precipitate formation was considered indicative of the absence of Phlobatannins when an aqueous crude methanol *Phragmanthera macrosolen L*. leaf extract of the sample was boiled with 5mL of 1% aqueous hydrochloric acid.

Proteins and amino acids tests
For the Biuret test, 0.5 mg of the *Phragmanthera macrosolen L*. leaf extract was mixed with an equal volume of 40% NaOH solution, and two drops of 1% copper sulfate solution were added. The development of a violet color signifies the presence of protein. In the Ninhydrin test, approximately 0.5 mg of the extract was taken, and 2 drops of freshly prepared 0.2% ninhydrin reagent were added before heating. The emergence of a pink color indicates the presence of proteins, peptides, or amino acids in *Phragmanthera macrosolen L*. leaf.

Preparation of *Phragmanthera macrosolen L*. Leaf

Phragmanthera macrosolen L. leaf was collected and cleaned systematically under running distilled water, then wetted carefully with ultra-purified water as well as dried at normal temperatures for seven days. Then the dried leaf was grounded by using a grinder to crush the leaf skins to a fine powder as shown in Fig. 1. The solutions of both leafs broth were prepared separately by taking 3 g leaf powder added to 100 ml deionized water and then boiling for 1 h at temperature of 70°C.

Then the leaf extract were cooled at room temperature for 24 h. Then the leaf extracts were filtered through What-man filter papers, and kept in a fridge-freezer for supplementary uses.

Bio-synthesis of Ag_2O NPs using *Phragmanthera macrosolen L*. leaf extracts

In the synthesis process, 1.67 g of $AgNO_3$ was dissolved in 80 ml of distilled water, rather than ethanol, to ensure optimal solubility and appropriate reaction conditions. Once the silver nitrate was completely dissolved, we proceeded by adding 20 ml of plant extract to the solution. The mixture was stirred continuously for 45 min at room temperature to guarantee uniform mixing and facilitate the interaction between the silver nitrate and the bioactive compounds in the extract as shown in Fig. 1. Interestingly, we observed that no additional base, such as NaOH or KOH, was required to initiate precipitation, as it occurred naturally during the reaction process. The pH of the solution was measured to be approximately 3.8, a slightly acidic environment that contributed to the successful formation of Ag_2O NPs. After precipitation formed the samples were washed using ethanol and distilled water several times. Then filtration followed by drying using oven at 90 °C for 4 h. This method, which utilizes the plant extract's reducing and stabilizing properties, allows for the green synthesis of nanoparticles without the need for harsh chemical agents. Finally, the samples were kept for supplementary characterization and applications.

Characterization techniques

The phytochemical analysis of the sample was analyzed using FTIR spectroscopy. Spectrum were verified to distinguish functional group elaborated in biosynthesized nanoparticle preparation and were attained through a Perkin Elmer FTIR spectro-photometer (Norwalk, CT, USA) at a resolution of 5/cm in a diffuse transmittance manner using potassium bromide (KBr) pellet. FIB-SEM and EDS was utilized to study the superficial morphology, size, and crystalline structure of the silver oxide nanoparticles. HR-TEM and SAED pattern (HR-TEM model, JEOL-2010, Japan) were utilized to check the surface morphology, sizes, and crystalline structures of the Ag_2O NPs. An optical property of material was analyzed using UV-Vis spectroscopy. X-ray diffractions of the nanoparticles were gained using a Rigaku X-ray diffraction meter (XRD) to investigate the crystalline phases of biosynthesized Ag_2O NPs.

Antibacterial assay

Agar well diffusion method
The antibacterial activity of Ag_2O NPs and *Phragmanthera macrosolen L*. leaf extract was done through an agar well diffusions technique[49]. The instruments that we use for disc diffusion and broth dilution are: Laminar airflow cabinet, Incubator, UV-Vis spectrophotometer, freezer, autoclave and hot air oven. In addition, we use many disposable items like 15 ml tubes, Petri dishes, spreaders, microfuge tubes and tips. The Mueller-Hinton

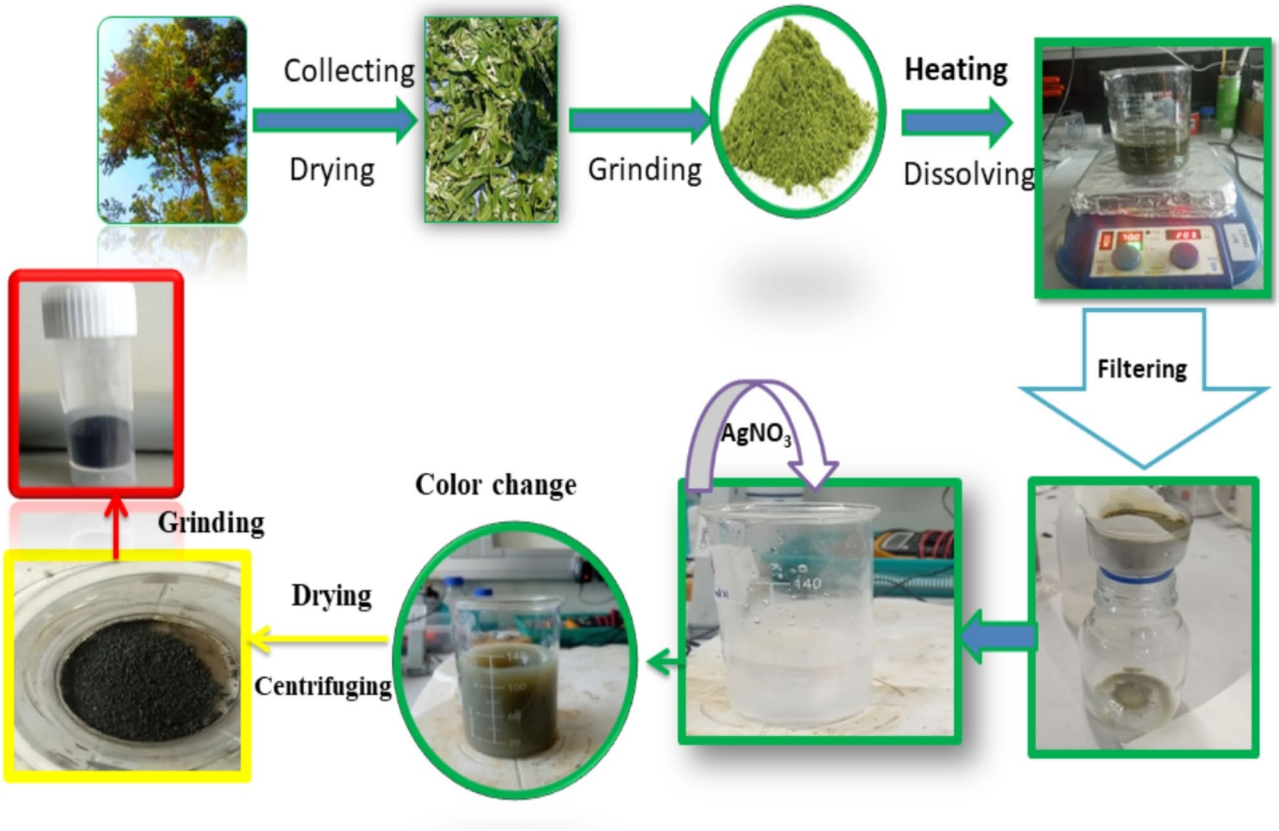

Figure 1. Green synthesis of Ag_2O NPs using *Phragmanthera macrosolen L.* leaf extract.

agar (MHA) mediums were equipped for anti-microbial tests since it is the finest mediums for emerging the furthermost pathogenic microorganisms. Two types of microbial bacterial strains: Gram-positive (*S. aureus)* and Gram-negative (*E. coli)* were used to investigate the anti-bacterial tests. To stimulates the microorganisms, they were grown-up in a richest medium cultures like as tryptic-soy-agar and nurtured at room temperature over-night for a nice sensitivity test. The microorganism's suspensions were moistened on the surface of the MHA underneath sterilized situations through the mopping approaches. Afterward the microorganisms desiccated up, made wells in the MHA with diameter of 6 mm. The well was penetrating with the bottom of sterilized indigo micro-pipette tips. The antimicrobial agents (Ag_2O NPs) are introduced into the wells using a micro-pipette. All the Bacterial straining were nurturing in dishes for 24 h. (it should not more than 24 h) at room temperature over-night. Lastly, the positively growing inhibition zones diameters around each well were recorded in millimeter.

Minimum inhibitory concentration

The testing substances demonstrated solubility in a 10% Dimethylsulfoxide (DMSO) solution. Initial test concentrations were arranged in 96-well plates, with each well receiving 5 µl of a sample containing 10^8 CFU/ml of bacteria. These plates were incubated at 37℃ for 24 h to observe bacterial growth. The culture potency of each well was recorded at 700 nm, referencing untreated controls. The MIC, representing the lowest nanoparticle concentrations, was identified, showcasing observable destruction of the test bacterial cultures[18,50].

Results and discussion

Phytochemical screening

Phytochemical screening is a qualitative test designed to assess the presence of active compounds in secondary metabolites within plant extracts, as outlined by[51]. The analysis involved obtaining samples of 80% ethanol extracts from *Phragmanthera macrosolen L.* leaf, each placed in a test tube. Subsequently, specific reagents were added corresponding to the identified compound groups, including flavonoids, alkaloids, Sesquiterpenoid Tests, tannins, Carbohydrates Tests, Phlobatannins, Proteins and amino acids. The qualitative analysis of the active compounds in the 80% ethanol extracts of *Phragmanthera macrosolen L.* plants is detailed in the accompanying Table 1 and FTIR anlysis displayed phytochemical test results through ethanol extract of *Phragmanthera macrosolen L.* leafs.

Compound Groups	Reagent	Color observed	Description
Flavonoids	Mg metal	Precipitate orange	y*
Alkaloids	Dragendorff, Mayer	Orange	y
Sesquiterpenoid	Diethyl ether	No	n
Carbohydrates	Fehling's	Yellow	y
Phlobatannins	Hydrochloric acid	No	n
Proteins, peptides, and amino acids	Copper sulfate	Pink	y*

Table 1. Displayed phytochemical test results through ethanol extract of *Phragmanthera macrosolen L.* leafs. Descriptions:. Symbol(y*): Contains more compounds (solid color) Symbol(y): contained less compound Symbol (n): no contained compound (no color formed)

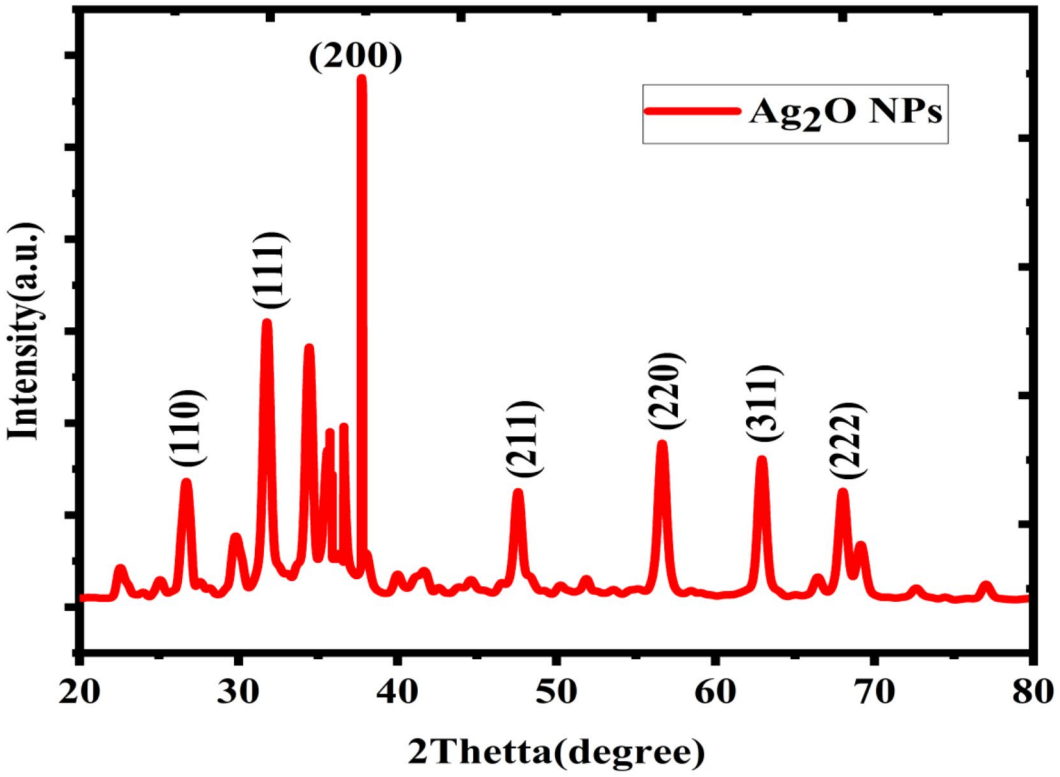

Figure 2. XRD pattern of Ag_2O NPs synthesized through *Phragmanthera macrosolen L.* leaf extract.

Structural study

The confirmation of crystal structure of the sample was studied utilizing Powder and bulk X-ray diffractometer (Rigaku Ultimate 1 V, Japan) with CuKα radiation sources (λ = 0.15417 nm) in 2θ ranges from 20 to 80°. The peaks intensities were ascertained via the locations of atoms within the lattice plane. The Scherer formula was applied to calculate crystalline size through use of XRD patterns that display line expansion[52,53]. In certain, the fine structures of extended x-ray absorptions might be used to detect small particles. Ag_2O NPs made through green approach were found to have XRD in the between 20° and 80° ranges. The XRD graph for Ag_2O NPs as synthesized Fig. 2 displayed intense peaks at 2θ = 26.447, 32.55, 37.764, 46.704, 54.48, 64.92 and 68.20° which can be indexed to the orientation planes (110), (111), (200), (211), (220), (311) and (222) respectively and agree with JCPDS no. 1393[18,54]. The result observed from SAED also confirmed as polycrystalline Ag_2O NPs formation[55]. The other observed peaks shown the presence of organic compounds from *Phragmanthera macrosolen L.* leaf extract which acted for the reductions of silver ion as well as stabilization of resultant nanoparticles[31,56].

The crystalline size of biosynthesized Ag_2O NPs were calculated using Debye-Scherer formula (Eq. 1) and XRD data plotted[23,57].

The crystallite parameters calculated from XRD and Scherer formula[58] displayed in Table 2.

2Thetta (degree)	FWHM (rad)	Crystalline Size(nm)	Dislocation density (δ)	Micro-strain (ϵ)	Lattice parameters (Å)
26.44	0.08873	85.18043	0.000138	0.000377	4.75
32.55	0.15302	48.70405	0.000422	0.000641	4.76
37.76	0.08786	83.61145	0.000143	0.000363	4.76
46.7	0.19124	37.27232	0.00072	0.000766	4.75
54.48	0.39354	17.54022	0.00325	0.001527	4.75
64.92	0.29555	22.16491	0.002035	0.001088	4.76
68.20	0.24412	26.33501	0.001442	0.000882	4.76

Table 2. Crystalline parameters calculated from XRD pattern of green synthesized Ag_2O NPs.

$$D\,(nm) = \frac{K\lambda}{\beta\, Cos\theta} \tag{1}$$

Where K is Scherer constant (typically around 0.9, but can vary depending on factors such as crystallite shape),
λ is the wavelength with CuKα radiation sources (λ = 0.15417 nm),
θ is the Bragg diffractions angles (peak positions) recorded from XRD peaks, and.
β is the full width at half maximum (FWHM) of the diffraction peaks recorded from XRD patterns.

Moreover, the structural parameters viz.; dislocation density (δ), and micro-strain(ε), lattice parameters were also computed from the XRD data using the formulae below. The dislocation density (δ) was computed using the following formula[59] and summarized in Table 1:

$$\delta = \frac{1}{D^2} \tag{2}$$

The micro-strain (ε) was computed using the following formula:

$$\epsilon = \frac{\beta\, cos\theta}{4} \tag{3}$$

The lattice parameters/constant (a) and (c) were computed using the following formula:

$$d_{(hkl)} = \frac{a}{\sqrt{h^2 + k^2 + l^2}} \tag{4}$$

In synthesized materials, the dislocation densities are in direct proportion to the micro-strains and inversely proportion to the crystalline size. The widening of diffraction peak occurs while atoms in crystals unit cell is emigrant from their own sites because of smaller crystalline size as well as the existence of lattice defect that might be measure dislocation densities[60]. The dislocations densities indicate the creations of imperfections and vacancy in the crystals. The smaller dislocation densities of nanoparticles shows the well compacted form of the materials[61]. The micro strains and crystalline size are extremely interrelated[62].

FTIR study

The phytochemical properties and functional groups of the synthesized *Phragmanthera macrosolen L.* and Ag_2O NPs are analyzed by FTIR spectrometer in the wave number ranges of 400–4000 cm^{-1}, as shown in Figs. 3 and 4 displayed the FTIR spectrums of Ag_2O NPs displayed a shift in bands associated to *Phragmanthera macrosolen L.* leaf extract and the possible mechanism of reduction of silver ion to form Ag_2O NPs. The phytochemical groups' alteration caused by addition of extract to $AgNO_3$ to prepare Ag_2O NPs. *Phragmanthera macrosolen L.* leaf extract displays several peaks of foremost phytochemical observed at 3351.58, 2861.19, 1475.37, 1147.31, 1027.61, 850 and 538 cm^{-1} which are categorized in Phenol rings groups, methyl group, C-C = C groups C-O, C-N stretch and -C-H bend correspondingly as shown in Table 3. These bioactive compounds might be involved in reducing the Ag^+ to Ag^0. The wide peak observed at 3351.58 cm^{-1} shows the high amount of existence of phenol rings which acted as reducing Ag^+ to Ag^0 in preparation of Ag_2O NPs. This phenol rings which contains flavonoids, alkaloids, tannins and essential oils[63] which can donate electron to the Ag^+ and reduces it to Ag^0; while Ag_2O NPs shows a shifts in the frequencies at 3467.91, 1610.44, 1364, 1021.44, 714, 595 and 500 cm^{-1}. All sharp and widening peaks agree to the enlarging vibrations of the hydroxyl groups (H-bonded-O-H-stretch), O-H meandering vibrations of an adsorbed water molecules on the surfaces of Ag_2O NPs, that might be needed for anti-microbial tests, and feeble extending vibrations, C = C correspondingly. Additionally, Ag_2O NPs shown Ag-O bending modes of vibrations at (500) cm^{-1}, approving metal-oxygen attachment formations[64].

UV-Visible absorption spectroscopy

The optical property of Ag_2O NPs was determined by UV-Vis spectrophotometer (PerkinElmer, Lambda 365, and Thailand). The reactions displayed initially, a whitish green color was gained and after two minutes, automatically the color changed to brownish black to confirm the reduction of silver ion. Uv-vis spectrum showed as Fig. 5 an absorption peak at 430 nm, confirming the synthesis of Ag_2O NPs. The wide higher absorption observed in the visible range of around 590.5 nm, which should be significantly activated in the visible light spectrum[56,67].

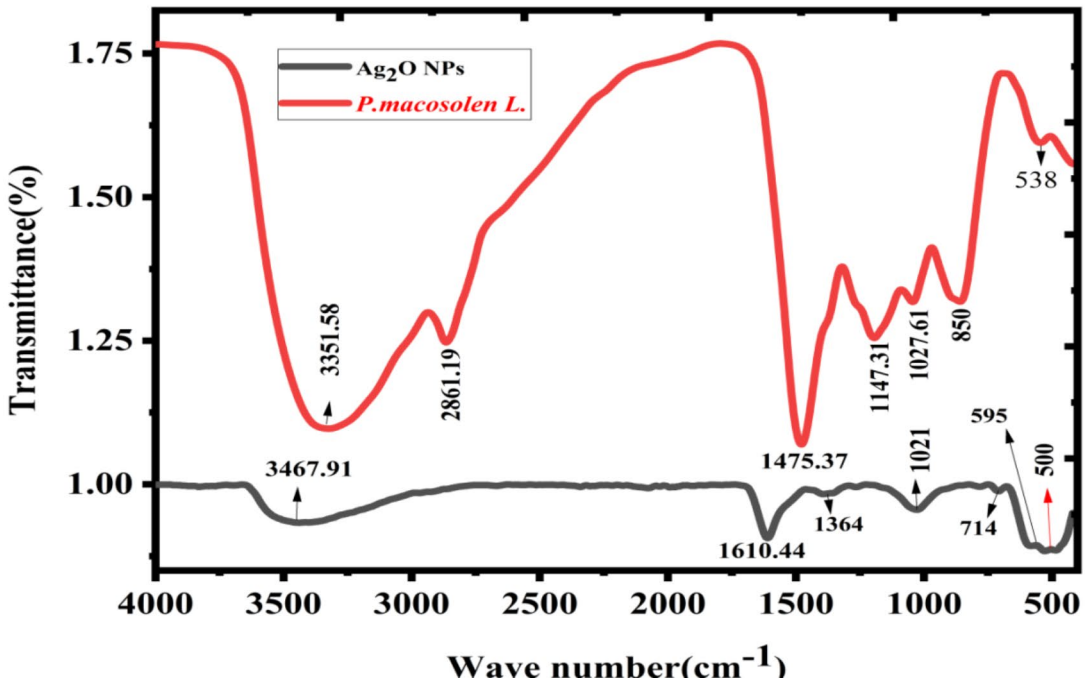

Figure 3. FTIR spectra of *Phragmanthera macrosolen L.* leaf powder and Ag_2O NPs powder synthesized by *Phragmanthera macrosolen L.* leaf.

To develop the programs in determination of the energy band gap by through the Tauc relation pilot used the data as an input. In this study we utilized wave length (λ) and absorption (A) which are attained from UV-Vis analysis, types of electron transitions (n), and (t) for the thickness of the sample. The Tauc relation pilot is initially presented by Tauch in 19s when he determined the band gap of amorphous Ge by through the data of absorptions spectra. This technique is grounded on assumptions that the energy is depending on absorption coefficients α[68]. It is then more modified by Davis as well as Mott for semi-conductor materials. They originate that optical absorption is based on the variance between photonic energy and energy band gap. The Tauc relation for semi-conductor material is expressed by Eq. (4)[69].

$$(\alpha\, hv)^{\gamma} = C(hv - Eg) \tag{5}$$

Where h is Plank's constant, *v* is photonic frequencies, *Eg* is energy band gap, C is proportionality constant, n is a factor which depending on electrons transition properties, and α is absorption coefficients[70]. The values of γ are ½ and 2 for direct as well as indirect energy band gap transitions, separately. The absorbance coefficient is calculated as Eq. (6)[71]

$$\alpha = \frac{\ln(10).A}{l} \tag{6}$$

Where A is absorptions and l is the thickness of the material in centimeters. The energy band gap by using Tauc relation is worked by plotting the values of $(\alpha\, hv)^{\gamma}$ verses hυ, as shown in Fig. 4 then by taking the extrapolations in the linear area crossways the energies axis in the consistent graphs. The inter-section with energy axis is the estimate of the respective energy band gap[72].

The energy gap calculated is 2.1 eV it confirms that the biosynthesized energy gap with direct transition. The obtained band gap is suitable for antimicrobial activity. Tauc pilot energy band gap of Ag_2O NPs was depicted in Fig. 5 (a) and (b) shown absorbance spectrums and Tauc pilot energy gap calculation. The calculated direct band gap (Eg) of Ag_2O NPs (2.1 eV) was found to be modified than the band gap value of bulk Ag_2O NPs. This modified in the band gap is attributed to the influence of native defects, which generate localized electronic states within the energy gap. Additionally, the band gap value significantly influences the photo-catalytic performance[72–75]. Consequently, this enhancement in absorption capabilities contributes to the improved photo-catalytic activity of Ag_2O NPs across these spectral regions.

The band gap of a material plays a crucial role in determining its light absorption characteristics and influences the wavelength at which antibacterial agents operate most effectively. In comparison, a wider band gap agent like bulk proves beneficial primarily at shorter wavelengths when compared to nanosized nanoparticles. Exciton binding energy, indicative of stability against thermal dissociation of exciton, becomes significant. A narrower

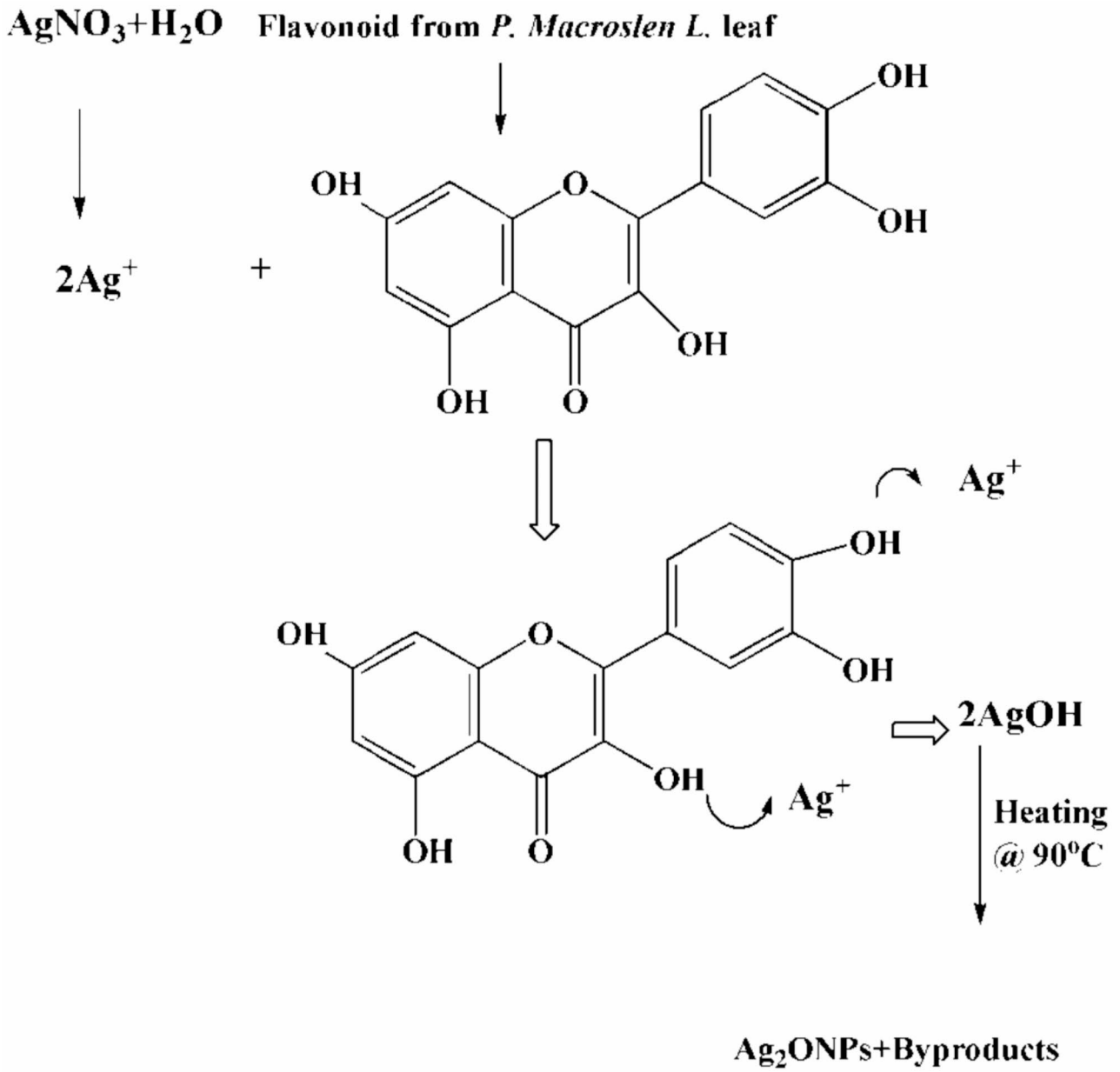

Figure 4. The possible mechanism of reduction of silver ions to form Ag_2O NPs by bioactive compounds.

band gap results in more free electrons and holes with sufficient lifetime, fostering the photo-generation of reactive oxygen species (ROS) on the nanoparticle's surface from adsorbed oxygen. Experimental findings emphasize the significant antibacterial performance of Ag_2O NPs at room temperature, owing to its narrower band gap[76,77].

SEM and EDS analysis

FIB-SEM metaphors of Ag_2O NPs have displayed in Fig. 6(a)-(c) and (d) which showed that surface morphology of the Ag_2O NPs are spherical and rod like of various sizes (40–80 nm) and mean particle size of Ag_2O NPs was determined to be 54.5 nm which also confirmed by XRD and HR-TEM results [78]. The FIB-SEM images shown agglomerations of individual Ag_2O NPs. A nearer looking at the agglomerated sphere and broken rod structures of Ag_2O NPs also displayed[79]. The EDS analysis approved out the existence of silver and oxygen in the sample using the spectrum peak taken as displayed in the Fig. 7. The elemental compositions study showed wide signal from silver regions and feebler signals from oxygen[80]. Furthermore, it is known from EDS study that the regular silver and oxygen amount in the sample was 72.07% and 27.93 by weight respectively.

TEM analysis

The wave-like behavior of electrons tunneling through Ag_2O NPs is depicted in the HR-TEM images presented in Fig. 8(a) and (b). These images unveil the spherical distribution of Ag_2O NPs within the powder sample, with

FTIR study of Phragmanthera macrosolen L.				Ref.
S. No.	Frequency (cm^{-1})	Bonds	Functional-groups	
1	3351.58	O-H stretching	Phenols	
2	2861.19	C-H bond	Alkane	
3	1475.34	C-C = C Asymmetric Stretch	Aromatic Rings	
4	1147.31	C–O	stretching assigned to the flavonoid groups	
5	1027.61	C-N stretch	Aliphatic amines	
6	850	= C-H bend		
7	538	C–Cl	stretching of alkyl halides	63–66
FTIR of Ag_2O NPs				
1	3467.91	O-H	Stretching of the alcohol, phenol group	
2	1610.44	N-H	bending group of 1^0 amines)	
3	1364	C–N	The stretching vibration of amide I bands proteins	
4	1021.44	C-N stretch	Aliphatic amines	
5	714	-C = C–H: C–H	bending of alkynes	
6	595	-C = C–H: C–H		
7	840 – 500	Ag-O		

Table 3. The phytochemical analysis *Phragmanthera Macrosolen L.* leaf and Ag_2O NPs from FTIR analysis.

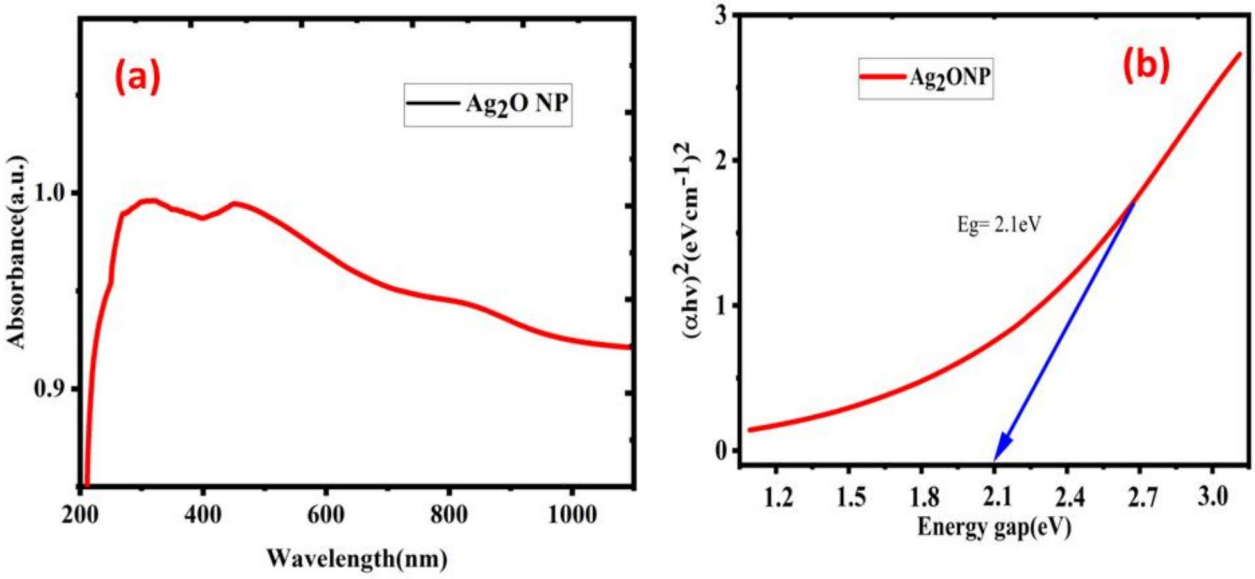

Figure 5. (**a**) Uv-Vis spectrum and (**b**). Tauc relation energy band gap of Ag_2O NPs by *P. macrosolen L.* leaf extract.

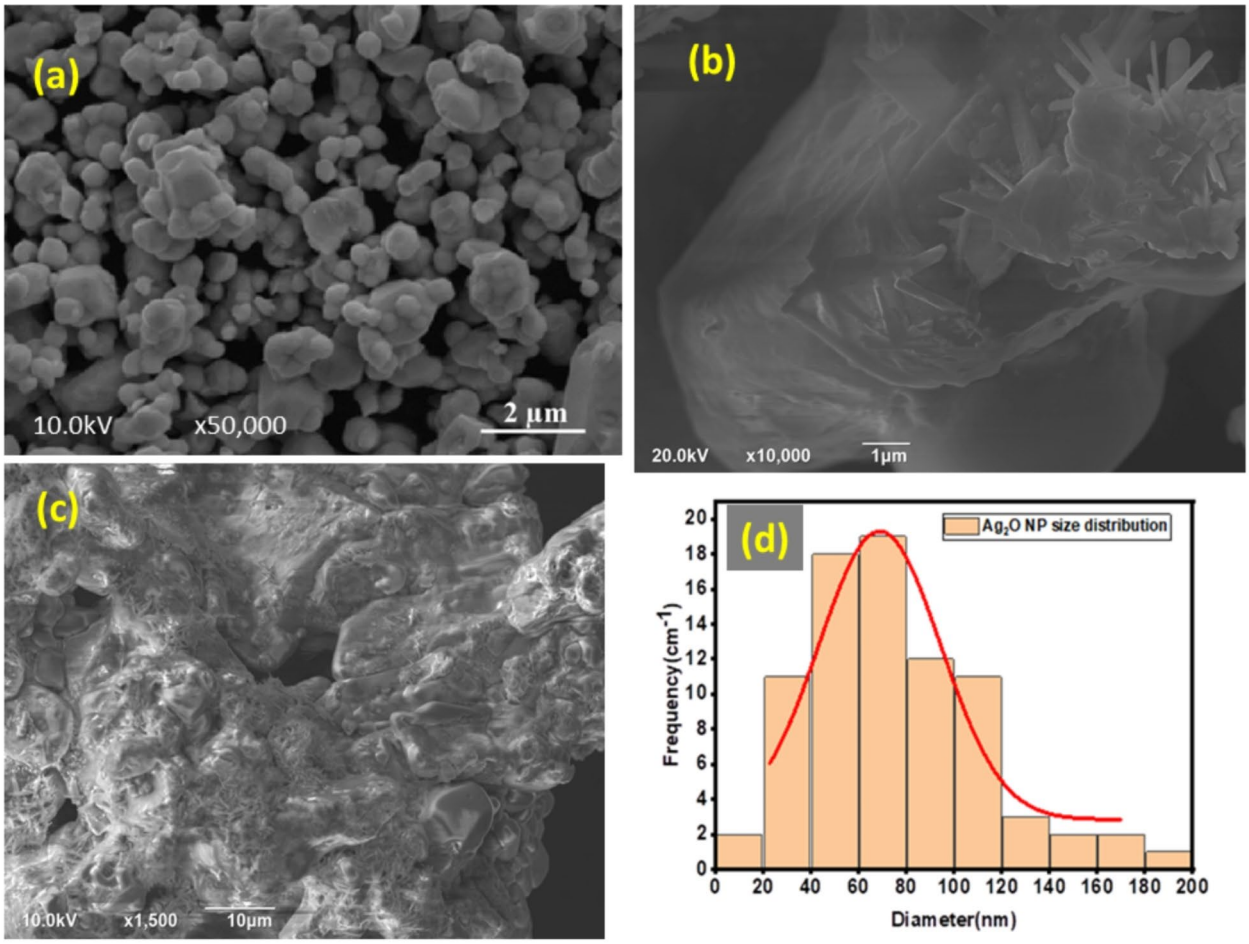

Figure 6. (**a**)-(**c**). FIB-SEM images of Ag_2O NPs taken on different magnification and position and (**d**). Particle size distribution.

observed sizes ranging from 20 nm to 80 nm. The particle size distribution graph illustrates a mean diameter of 45.87 nm for the Ag_2O NPs which also confirmed by XRD and FIB-SEM results Fig. 8(c). Additionally, Fig. 8(d) demonstrates the poly-crystalline nature of the Ag_2O NPs, confirming this characteristic through the presence of bright circular spots in the obtained SAED patterns[81].

Antibacterial activity of Ag2O NPs

The synthesized Ag_2O NPs using *Phragmanthera macrosolen* L. leaf extracts demonstrated notable antibacterial effects, with inhibition zones varying depending on the concentration and volume of the tested sample solution. The antibacterial activity was evaluated against two bacterial strains, *E. coli* (gram-negative) and *S. aureus* (gram-positive), using different concentrations of Ag_2O NPs (20 mg/ml and 10 mg/ml). Each concentration was tested with sample volumes of 3.75, 7.5, 15, 30, 45, and 60 µl.

The inhibition zones for *E. coli* increased with the volume and concentration of the Ag_2O NPs[30,82]. For 20 mg/ml samples, the inhibition zones were 40 mm, 37 mm, 35 mm, and 34 mm for 60, 45, 30, and 15 µl, respectively, with no inhibition observed for 3.75 and 7.5 µl. For 10 mg/ml, the inhibition zones were 28 mm, 26 mm, 23 mm, and 22 mm at the corresponding sample volumes, with no inhibition detected for 3.75 and 7.5 µl. This data is represented in Fig. 9(a-h) and Table 4(a) and (b), illustrating the results for *E. coli* and *S. aureus*.

Similarly, for *S. aureus*, the 20 mg/ml Ag_2O NPs resulted in inhibition zones of 30 mm, 29 mm, 26 mm, and 24 mm for 60, 45, 30, and 15 µl, with no inhibition for 7.5 and 3.75 µl. The 10 mg/ml sample showed inhibition zones of 28 mm, 25 mm, 24 mm, and 20 mm. The results indicate a clear trend of increased antibacterial activity with higher sample concentrations and volumes[83].

The Ag_2O NPs exhibited greater antibacterial activity against *E. coli* than *S. aureus*, with the highest inhibition zone of 40 mm observed for 60 µl of the 20 mg/ml Ag_2O NPs solution against *E. coli*. The highest inhibition zone for *S. aureus* was 30 mm at the same concentration and volume. At the lower concentration (10 mg/ml), the highest inhibition zones for *E. coli* and *S. aureus* were 29 mm and 28 mm, respectively[84].

The superior antibacterial activity of Ag_2O NPs can be attributed to their ability to generate reactive oxygen species (ROS), which cause oxidative stress and damage to bacterial proteins and DNA[25,85]. The interaction of Ag_2O NPs with sulfur and phosphorus in bacterial DNA disrupts cell replication, leading to cell death[86]. This

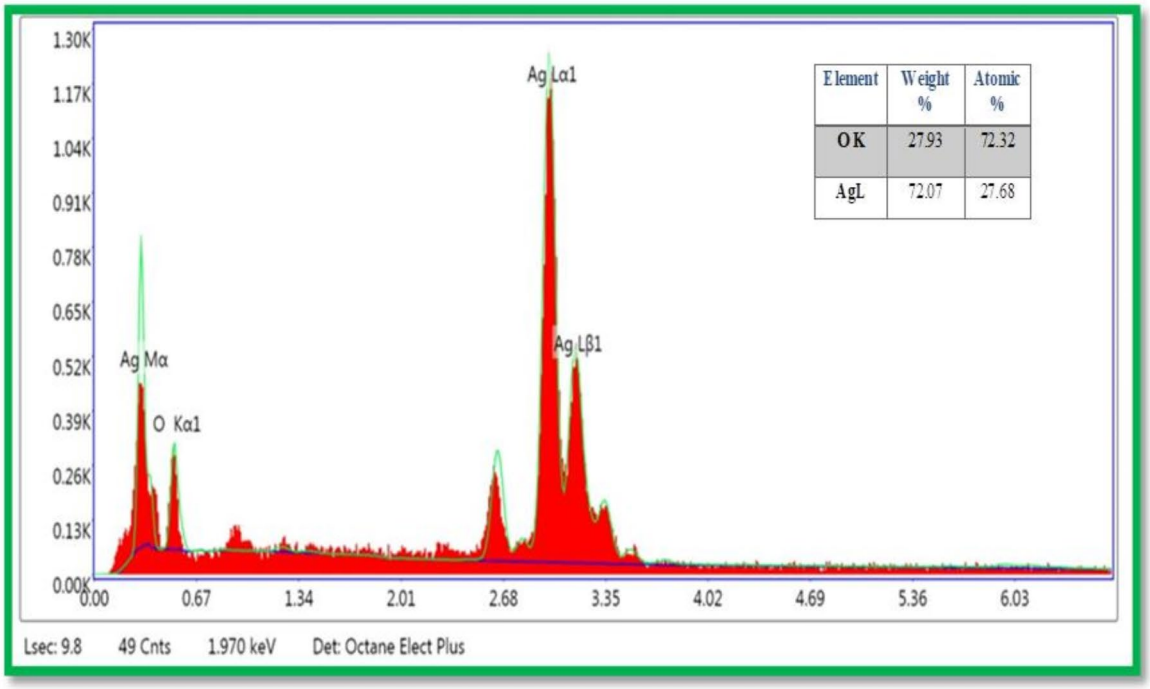

Figure 7. EDS Elemental Analysis of Ag_2O NPs using *Phragmanthera macrosolen L.* leaf extract.

mechanism is likely responsible for the observed antibacterial effects, particularly against *E. coli*, as depicted in Figs. 9 and 10, and Fig. 11.

The antibacterial efficacy of green-synthesized Ag_2O NPs was compared with other metal oxides synthesized by various methods, as shown in Table 5. Metal oxides such as ZnO, TiO_2, CuO, and Fe_3O_4 have been widely studied for their antibacterial properties. However, the inhibition zones observed in these metal oxides are generally lower than those exhibited by the green-synthesized Ag_2O NPs in this study. For instance, ZnO NPs synthesized through sol-gel methods typically produce inhibition zones in the range of 15–20 mm against *E. coli* and *S. aureus*[87], while CuO NPs, prepared via hydrothermal techniques, display zones between 18 and 22 mm[88]. In contrast, the green-synthesized Ag_2O NPs in the current study achieved inhibition zones as high as 40 mm against *E. coli* and 30 mm against *S. aureus*, highlighting their superior antibacterial activity. The enhanced antibacterial performance of the green-synthesized Ag_2O NPs can be attributed to the environmentally friendly synthesis process, which utilizes plant extracts that act as reducing and stabilizing agents. This method likely produces nanoparticles with a more reactive surface, thereby increasing their interaction with bacterial cells. Furthermore, the smaller particle size and the production of reactive oxygen species (ROS) by Ag_2O NPs contribute to their higher antibacterial efficacy[33]. In comparison, other metal oxides, though effective, often show reduced inhibition zones, possibly due to their larger particle sizes or the lack of ROS generation[89]. Thus, the green synthesis of Ag_2O NPs offers a promising alternative, not only for its eco-friendly approach but also for its enhanced antibacterial potential.

Minimum inhibitory concentration (MIC) for the biosynthesized Ag2O NPs

The Minimum Inhibitory Concentration (MIC) method was employed to assess the inhibitory effect of Ag_2O NPs on pathogenic organisms, demonstrating their adverse impact. Serial dilutions ranging from 60 to 3.75 µg/ml were deliberately applied, determining the minimum concentration at which antibacterial properties were still evident. The concentrations for *S. aureus* and *E. coli* were found to be 15 and 30 µg respectively for both 10 g/ml and 20 mg/ml. The results indicate that Ag_2O NPs biosynthesized from *Phragmanthera macrosolen L.* leaf extract effectively inhibit the growth of certain bacteria at lower concentrations. All experiments were conducted in triplicate, and error bars in the form of standard deviation are presented in the data[42]. MIC as well as MBC is generally utilized to estimate the capability of antibacterial agents. After testing, it could be decided

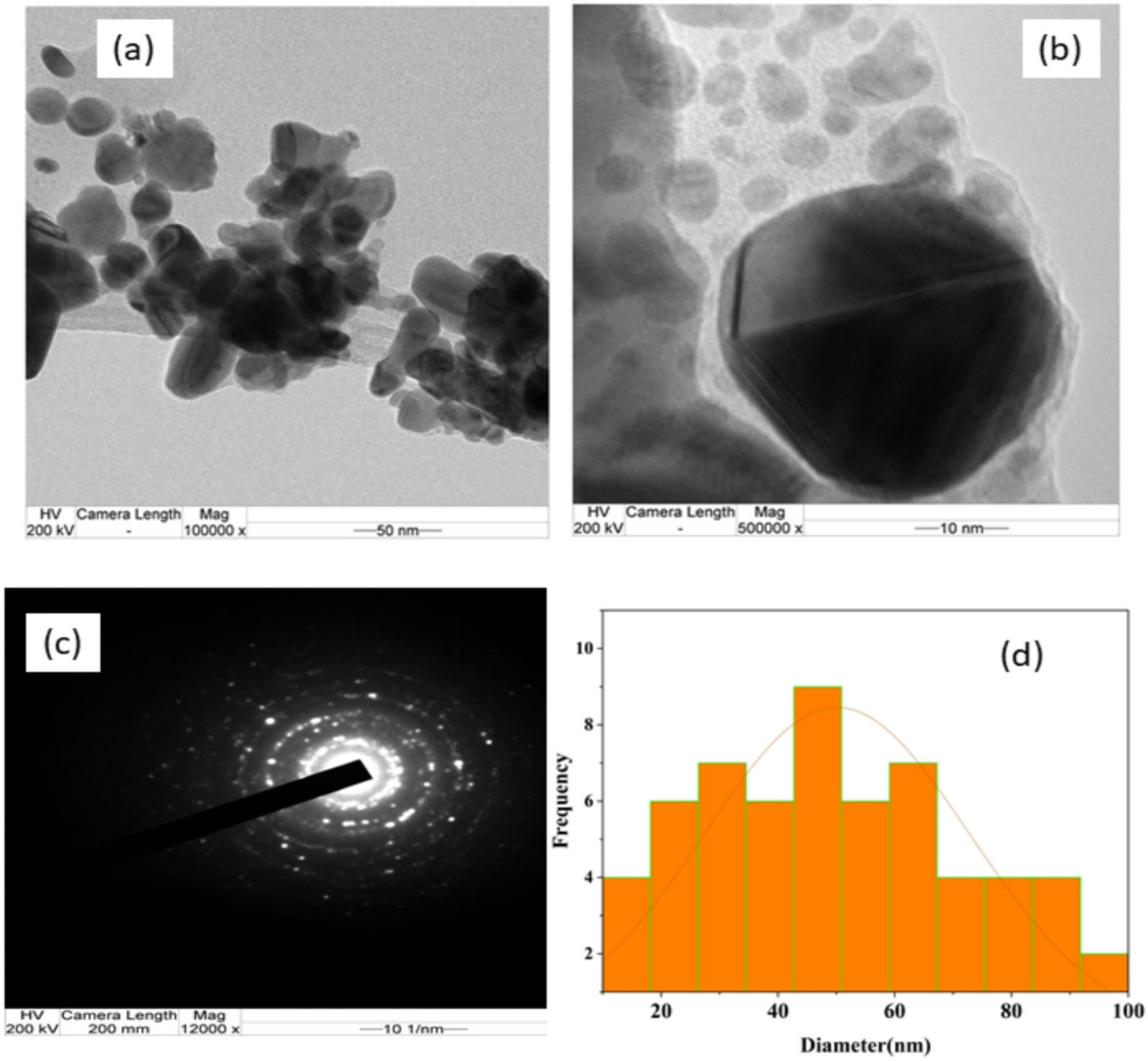

Figure 8. HR-TEM image (**a**) and (**b**) at different magnification (**c**) SAED image and (**d**) histogram particle size distribution analysis of biosynthesized Ag_2O NPs using *Phragmanthera macrosolen L.* leaf extract.

that as synthesized Ag_2O NPs gave the MIC of 15 µg/ml and 30 µg/ml much lesser than that of commercially existing particles which gave the MIC of about 800 µg/ml, while the MBC was 30 µg/ml powerfully evidencing the advantages of the quite little using dosage[98].

Conclusion

Silver oxide (Ag_2O) nanoparticles were successfully synthesized using a green method involving the crude extract of *Phragmanthera macrosolen L.* which is cost effective and eco-friendly. The prepared Ag_2O nanoparticles characterized through techniques such as SEM, HR-TEM, XRD, FTIR Spectroscopy, EDS, and UV-Vis Spectrometry. All characterization made reveals that the Ag_2O NPs are suitable for antibacterial activity. The nanosized biosynthesized Ag_2O nanoparticles, derived from the leaves of *Phragmanthera macrosolen L.*, exhibited notable antibacterial activity, particularly against strains of *S. aureus* and *E. coli*. The investigation into antimicrobial efficacy indicated that Ag_2O nanoparticles displayed superior effectiveness against these bacterial strains than those synthesized by chemical and physical techniques. The bioactive compounds available in crude leaf extracts of *Phragmanthera macrosolen L.* used as reducing, capping and stabilizing agents during formation of Ag_2O NPs by donating ions. These findings suggest that biosynthesized Ag_2O NPs might serve as highly potent antimicrobial agents against pathogens, making them potentially valuable for various medicinal applications.

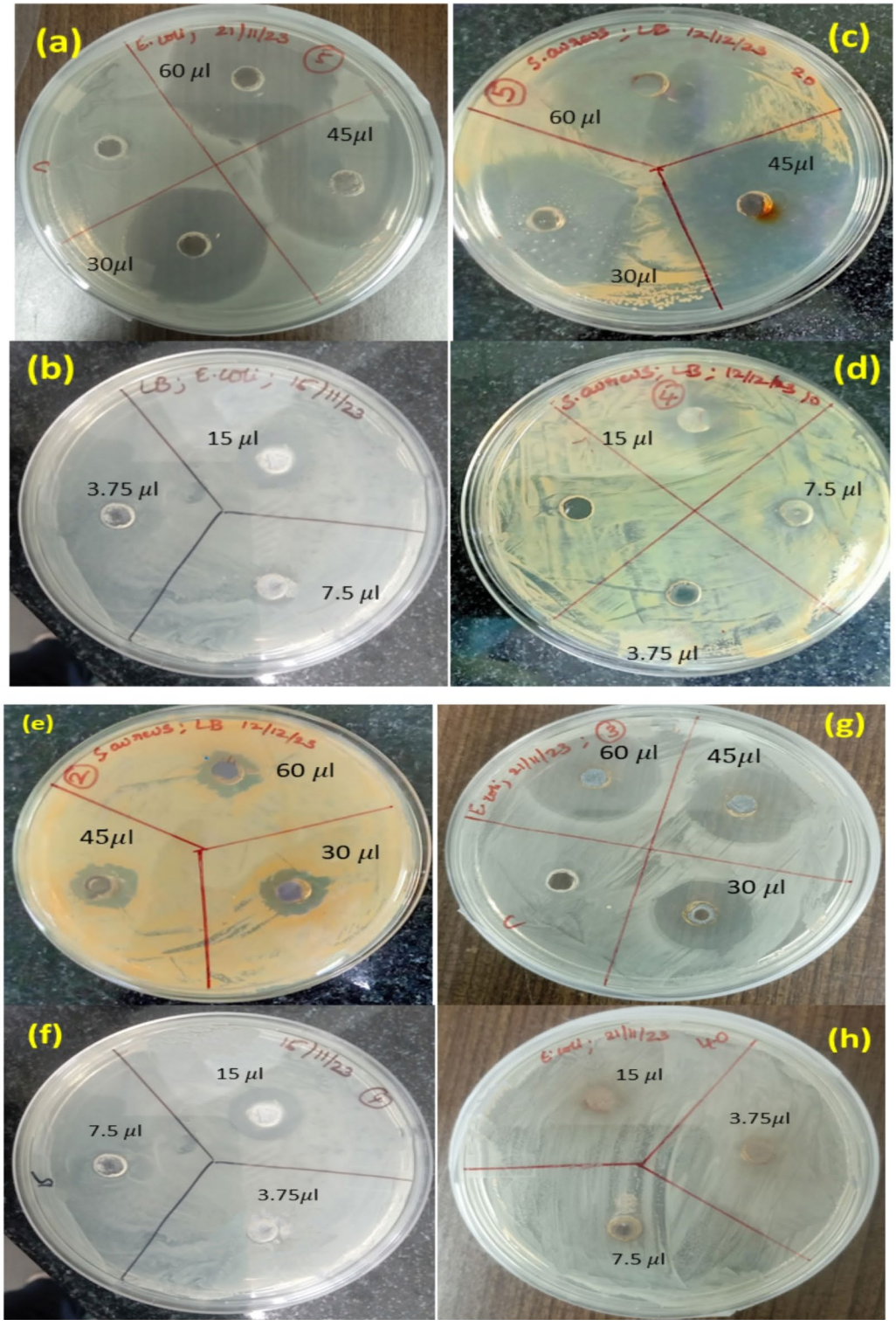

Figure 9. Inhibition zones of Antibacterial activity of Ag_2O NPs against *E. coli* and *S. aureus* by the disc diffusion method at different concentrations.

(a) 20 mg/ml of the samples and						
Bacterial strain	**Zone of Inhibition(mm)**					
	3.75µl	**7.5µl**	**15µl**	**30µl**	**45µl**	**60µl**
E.coli	0	0	34	35	37	40
S. aureus	0	0	27	29	31	30
Control	-	-	-	-	-	-
(b) 10 mg/ml of samples						
Bacterial strain	**Zone of Inhibition(mm)**					
	3.75µl	**7.5µl**	**15µl**	**30µl**	**45µl**	**60µl**
E.coli	0	0	22	23	26	29
S. aureus	0	0	20	24	25	28
Control	-	-	-	-	-	-

Table 4. Antibacterial activity of biosynthesized Ag_2O NPs via *Phragmanthera Macrosolen L.* leaf for.

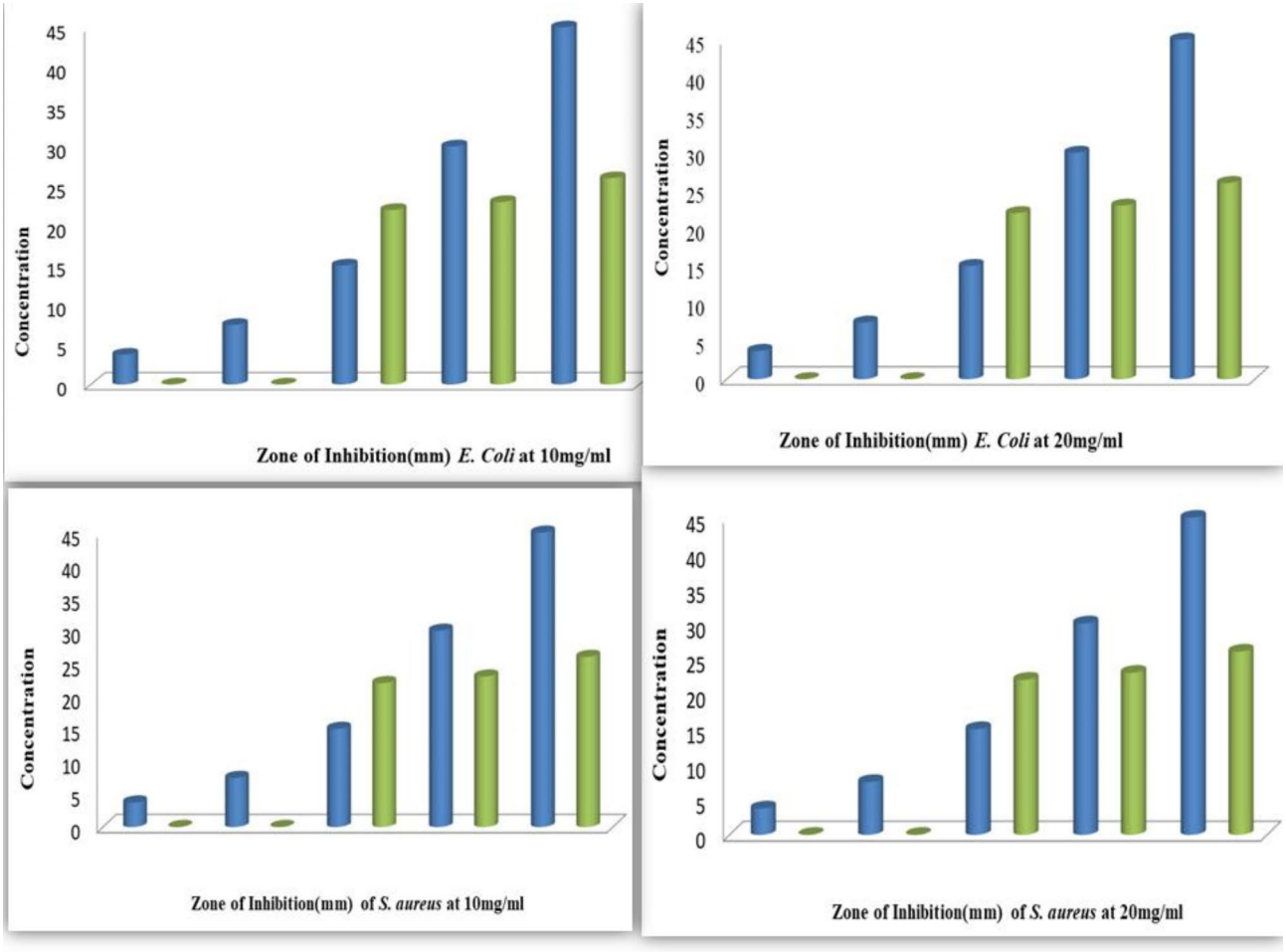

Figure 10. Comparison of zones of inhibition (ZOI) of E. *coli* and *S. aureus* at different concentrations.

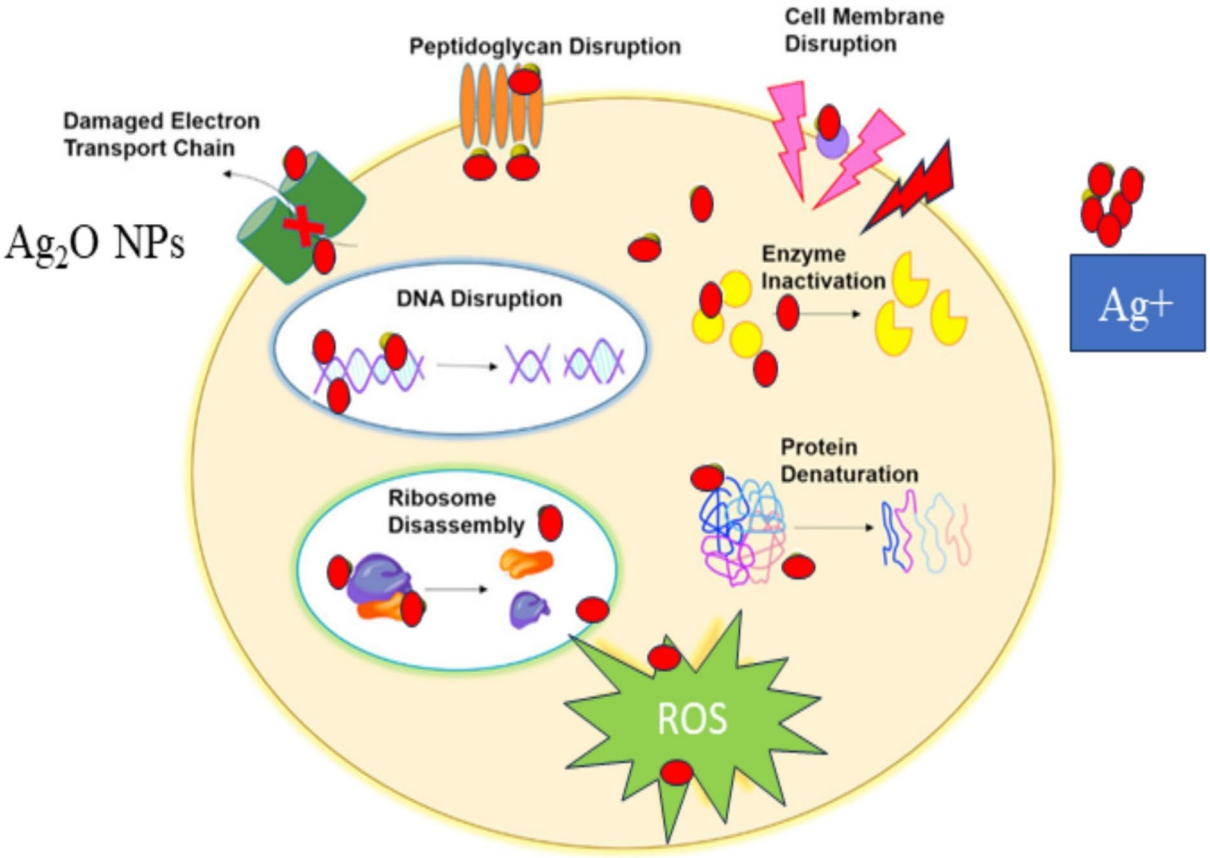

Figure 11. Possible mechanism of antibacterial activity of Ag_2O NPs against bacterial strains.

Metal Oxide NPs	Synthesis Method	Bacterial Strains	Inhibition Zone(mm)	References
CuO NPs	Green synthesis	*E. coli and S. aureus*	35 and 0	90
CuO NPs	Laser Production	*E. coli* and *S. aureus*	16.5 and 15	91
Fe_2O_3 NPs	Biosynthesis	*E. coli* and *S. aureus*	10 and 8	92
TiO_2NPs	Sol-gel	*E. Coli*, *K. pneumoniae* and *B. subtilis*	12.50, 18.75 and 18.75	93
MgO NPs	Ultrasonic-Assisted Sol-Gel Method	*S. aureus*, *E. coli* and *C. albicans*	19.3, 16.1 and 15.2	94
NiO NPs	photolysis method	*Klebsiella* and *E. coli*	14 and 16	95
MnO_2NPs	Green synthesis	*S. aureus*, *E. coli* and *P. aeruginosa*	22, 18 and 15	96
CeO_2NPs	Biosynthesis	*S. aureus* and *E. coli.*	22 and 19	97
Ag_2O NPs	Green synthesis	*S. aureus* and *E. coli*	30 and 40	This Work

Table 5. Comparisons of metal oxides and the green synthesized Ag_2O NPs.

Data availability

The datasets used and analyzed during the current study are available from the corresponding author on request.

Received: 24 December 2023; Accepted: 3 October 2024
Published online: 06 November 2024

References

1. Deepa, C., Rajeshkumar, L. & Ramesh, M. Preparation, synthesis, properties and characterization of graphene-based 2D nanomaterials for biosensors and bioelectronics. *J. Mater. Res. Technol.* **19**, 2657–2694 (2022).
2. Reyes-Carmona, L., Camps, E., Campos-González, E., Mercado-Celis, G., Cervantes-Garduño, A., Pérez-Ibarra, E. A., ... & Almaguer-Flores, A. Antimicrobial evaluation of bismuth subsalicylate nanoparticles synthesized by laser ablation against clinical oral microorganisms. *Opt. Laser Technol.* **158**, 108930 (2023).

3. Saka, A., Jule, L. T., Badassa, B., Gudata, L., Nagaprasad, N., Shanmugam, R., ... & Ramaswamy, K. Biosynthesis of TiO2 nano particles by using Rosemary (Rosmarinus officinalis) leaf extracts and its application for crystal dye degradation under sunlight. *BMC Chemistry*, **18**(1), 123 (2024).
4. Danish, M. S. S. et al. Photocatalytic applications of metal oxides for sustainable environmental remediation. *Met. (Basel)*. **11**, 1–25 (2021).
5. Saka, A., Tesfaye, J. L., Gudata, L., Shanmugam, R., Dwarampudi, L. P., Nagaprasad, N., ... & Rajeshkumar, S. Synthesis, characterization, and antibacterial activity of ZnO nanoparticles from fresh leaf extracts of Apocynaceae, Carissa spinarum L.(Hagamsa). *J. Nanomater*. **2022**(1), 6230298 (2022).
6. Huang, K. et al. Recent advances on silver-based photocatalysis: photocorrosion inhibition, visible-light responsivity enhancement, and charges separation acceleration. *Sep. Purif. Technol.* **283**, 120194 (2022).
7. Abel, S. et al. Biobutanol preparation through sugar-rich biomass by Clostridium saccharoperbutylacetonicum conversion using ZnO nanoparticle catalyst. *Biomass Convers. Biorefinery*. https://doi.org/10.1007/s13399-022-02424-1 (2022).
8. Shume, W. M., Murthy, H. A., & Zereffa, E. A. A review on synthesis and characterization of Ag2O nanoparticles for photocatalytic applications. *J. Chem*. **2020**(1), 5039479 (2020).
9. Raj, S., Trivedi, R., & Soni, V. Biogenic synthesis of silver nanoparticles, characterization and their applications—a review. *Surfaces* **5**(1), 67–90 (2021).
10. Sreenivas, B. et al. Synthesis and characterization of ZnO, ZnO Doped Ag2O nanoparticles and its photocatalytic activity. *Curr. Mater. Sci.* **16**, 826–833 (2023).
11. Sultan, A. E., Abdullah, H. I. & Niama, A. H. Synthesis of silver oxide nanoparticles using different precursor and study cytotoxicity against MCF-7 breast Cancer Cell line. *Nanomed. Res. J.* **8**, 259–267 (2023).
12. Gudkov, S. V., Li, R., Serov, D. A., Burmistrov, D. E., Baimler, I. V., Baryshev, A. S., ... & Lednev, V. N. Fluoroplast doped by Ag2O nanoparticles as new repairing non-cytotoxic antibacterial coating for meat industry. *Int. J. Mol. Sci*. **24**(1), 869 (2023).
13. Shivanna, S., Purushotham, D., Kodandaram, A. & Nagabhushana, C. M. Mavinakere Ramesh, A. Microwave assisted hydrothermal synthesis of Ag2O/α-Bi2O3 heterostructures with highly enhanced photocatalysis and their environmental interest. *Chem. Phys. Impact*. **6**, 100241 (2023).
14. Sirimekanont, T., Supaphol, P. & Sombatmankhong, K. Titanium (IV) oxide composite hollow nanofibres with silver oxide outgrowth by combined sol–gel and electrospinning techniques and their potential applications in energy and environment. *Adv. Compos. Hybrid. Mater.* **6**, 1–19 (2023).
15. Merckel, R. D. (2020). The impact of oxygen exothermicity on energy quality of biofuels and catalytic upgrading. University of Pretoria **53**, 1689–1699 (2019).
16. Abel, S., Tesfaye, J. L., Nagaprasad, N., Shanmugam, R., Dwarampudi, L. P., & Krishnaraj, R. Synthesis and characterization of zinc oxide nanoparticles using moringa leaf extract. *J. Nanomater*. **2021**(1), 4525770 (2021).
17. Parauha, Y. R., Sahu, V. & Dhoble, S. J. Prospective of combustion method for preparation of nanomaterials: a challenge. *Mater. Sci. Eng. B.* **267**, 115054 (2021).
18. Fayyadh, A. A. & Jaduaa Alzubaidy, M. H. Green-synthesis of Ag2O nanoparticles for antimicrobial assays. *J. Mech. Behav. Mater.* **30**, 228–236 (2021).
19. Li, R. et al. Biosynthesis of silver oxide nanoparticles and their photocatalytic and antimicrobial activity evaluation for wound healing applications in nursing care. *J. Photochem. Photobiol B Biol.* **199**, 111593 (2019).
20. Ismail, H. H., Hasoon, S. A. & Saheb, E. J. The anti- leishmaniasis activity of green synthesis silver oxide nanoparticles. *Ann. Trop. Med. Public. Heal.* **22**, (2019).
21. Aisida, S. O. et al. Biosynthesis of silver oxide nanoparticles using leave extract of Telfairia Occidentalis and its antibacterial activity. *Mater. Today Proc.* **36**, 208–213 (2019).
22. Sundararajan, G. Green Synthesis and characterization of silver oxide nanoparticles using Plant Extract volume. *Appl. Sci. Comput.* **VI**, 987–1004 (2019).
23. Belaiche, Y. et al. Green synthesis and characterization of silver/silver oxide nanoparticles using aqueous leaves extract of artemisia herba-alba as reducing and capping agents. *Rev. Rom Mater. Rom J. Mater.* **51**, 342–352 (2021).
24. Rashmi, B. N. et al. Facile green synthesis of silver oxide nanoparticles and their electrochemical, photocatalytic and biological studies. *Inorg. Chem. Commun.* **111**, 107580 (2020).
25. Shahzad Shirazi, M. et al. Bioengineered synthesis of phytochemical-adorned green silver oxide (Ag2O) nanoparticles via Mentha pulegium and Ficus carica extracts with high antioxidant, antibacterial, and antifungal activities. *Sci. Rep.* **12**, 1–15 (2022).
26. Maheshwaran, G. et al. Green synthesis of silver oxide nanoparticles using Zephyranthes Rosea flower extract and evaluation of biological activities. *J. Environ. Chem. Eng.* **8**, 104137 (2020).
27. Abbasi, B. A. et al. Environmentally friendly green approach for the fabrication of silver oxide nanoparticles: characterization and diverse biomedical applications. *Microsc Res. Tech.* **83**, 1308–1320 (2020).
28. Aiswariya, K. S. & Jose, V. Bioactive molecules Coated Silver Oxide Nanoparticle synthesis from Curcuma zanthorrhiza and HR-LCMS monitored validation of its photocatalytic potency towards Malachite Green Degradation. *J. Clust Sci.* **33**, 1685–1696 (2022).
29. Velsankar, K., Parvathy, G., Sankaranarayanan, K., Mohandoss, S. & Sudhahar, S. Green synthesis of silver oxide nanoparticles using Panicum miliaceum grains extract for biological applications. *Adv. Powder Technol.* **33**, 103645 (2022).
30. Pradheesh, G., Suresh, S., Suresh, J. & Alexramani, V. Antimicrobial and anticancer activity studies on Green Synthesized Silver Oxide nanoparticles from the Medicinal Plant Cyathea Nilgiriensis Holttum. *Int. J. Pharm. Investig.* **10**, 146–150 (2020).
31. Dharmaraj, D., Krishnamoorthy, M., Rajendran, K., Karuppiah, K., Annamalai, J., Durairaj, K. R., ... & Ethiraj, K. Antibacterial and cytotoxicity activities of biosynthesized silver oxide (Ag2O) nanoparticles using Bacillus paramycoides. *Journal of Drug Delivery Science and Technology* **61**, 102111 (2021).
32. Vinay, S. P., Udayabhanu, Nagaraju, G., Chandrappa, C. P. & Chandrasekhar, N. Novel Gomutra (cow urine) mediated synthesis of silver oxide nanoparticles and their enhanced photocatalytic, photoluminescence and antibacterial studies. *J. Sci. Adv. Mater. Devices.* **4**, 392–399 (2019).
33. Gudkov, S. V., Serov, D. A., Astashev, M. E., Semenova, A. A. & Lisitsyn, A. B. Ag2O nanoparticles as a candidate for Antimicrobial compounds of the New Generation. *Pharmaceuticals.* **15**, 1–22 (2022).
34. Elemike, E. E., Onwudiwe, D. C., Ekennia, A. C., Sonde, C. U. & Ehiri, R. C. Green synthesis of Ag/Ag2O nanoparticles using aqueous leaf extract of Eupatorium odoratum and its antimicrobial and mosquito larvicidal activities. *Molecules*. **22**, 1–15 (2017).
35. Zhang, J., Liu, H. & Ma, Z. Flower-like Ag2O/Bi2MoO6 p-n heterojunction with enhanced photocatalytic activity under visible light irradiation. *J. Mol. Catal. Chem.* **424**, 37–44 (2016).
36. Gaikwad, S. S. & Choudhari, V. P. Efficacy and Safety of Combination Therapy of Zinc and Silver Oxide nanoparticles in Streptozotocin-Induced Diabetic rats. *Int. J. Pharm. Res. Allied Sci.* **11**, 1–10 (2022).
37. Lee, S. H. & Jun, B. H. Silver nanoparticles: synthesis and application for nanomedicine. *Int. J. Mol. Sci.* **20**, (2019).
38. Thahira Khatoon, U., Velidandi, A., Rao, G. V. & S, N. Silver oxide nanoparticles: synthesis via chemical reduction, characterization, antimicrobial, and cytotoxicity studies. *Inorg. Chem. Commun.* **159**, 111690 (2024).
39. Thakur, P. K. & Verma, V. A. Review on Green Synthesis, characterization and anticancer application of metallic nanoparticles. *Appl. Biochem. Biotechnol.* **193**, 2357–2378 (2021).

40. Abel, S., Tesfaye, J. L., Shanmugam, R., Dwarampudi, L. P., Lamessa, G., Nagaprasad, N., ... & Krishnaraj, R. Green synthesis and characterizations of zinc oxide (ZnO) nanoparticles using aqueous leaf extracts of coffee (Coffea arabica) and its application in environmental toxicity reduction. *J. Nanomater*. **2021**(1), 3413350 (2021).
41. Diver, D., Nhapi, I. & Ruziwa, W. R. The potential and constraints of replacing conventional chemical coagulants with natural plant extracts in water and wastewater treatment. *Environ. Adv.* **13**, 100421 (2023).
42. Wang, Y. et al. Green synthesis of nanoparticles for the remediation of contaminated waters and soils: constituents, synthesizing methods, and influencing factors. *J. Clean. Prod.* **226**, 540–549 (2019).
43. Muche, M., Muasya, A. M. & Tsegay, B. A. Biology and resource acquisition of mistletoes, and the defense responses of host plants. *Ecol. Process.* **11**, (2022).
44. Shubham, S., Mishra, R., Gautam, N., Nepal, M., Kashyap, N., & Dutta, K. Phytochemical analysis of papaya leaf extract: screening test. *EC Dental Science* **18**(3), 485–490 (2019).
45. Eby Juliana Sabrima1, Sanjaya, R. & Surmiasih, Y. D. S. *Biomedical J. Indonesia* **6**, 357–363 (2020).
46. Wu, C. C., Huang, S. L., Ko, C. H. & Chang, H. T. Antifungal sesquiterpenoids from Michelia Formosana Leaf essential oil against Wood-rotting Fungi. *Molecules*. **27**, 1–8 (2022).
47. Nortjie, E., Basitere, M., Moyo, D., & Nyamukamba, P. Extraction methods, quantitative and qualitative phytochemical screening of medicinal plants for antimicrobial textiles: a review. *Plants*, **11**(15), 2011 (2022).
48. Shah, S. W. A. & heavy metals and antimicrobial activities of leaf, stem and roots extracts oF. In-vitro evaluation of phytochemicals, Caltha palustris var. alba. *J. Chil. Chem. Soc.* **68**, 5807–5812 (2023).
49. Álvarez-Chimal, R. et al. Influence of the particle size on the antibacterial activity of green synthesized zinc oxide nanoparticles using Dysphania ambrosioides extract, supported by molecular docking analysis. *Arab. J. Chem*. **15**, (2022).
50. Li, R. et al. Journal of Photochemistry Biology Biosynthesis of silver oxide nanoparticles and their photocatalytic and antimicrobial activity evaluation for wound healing applications in nursing care. *J. Photochem. Photobiol. B Biol.* 199, 111593 (2019).
51. Farag, R. S., Abdel-Latif, M. S., Baky, A. E., Tawfeek, L. S. & H. H. & Phytochemical screening and antioxidant activity of some medicinal plants' crude juices. *Biotechnol. Rep.* **28**, e00536 (2020).
52. Jeung, D. G., Lee, M., Paek, S. M. & Oh, J. M. Controlled growth of silver oxide nanoparticles on the surface of citrate anion intercalated layered double hydroxide. *Nanomaterials*. **11**, 1–16 (2021).
53. Ibrahim, H. M. M. Green synthesis and characterization of silver nanoparticles using banana peel extract and their antimicrobial activity against representative microorganisms. *J. Radiat. Res. Appl. Sci.* **8**, 265–275 (2015).
54. Yang, L., Hu, Y., Su, M. & Zhang, L. Fabrication of Dandelion-like p-p type heterostructure of Ag2O@CoO for Bifunctional Photoelectrocatalytic performance. *Langmuir*. **36**, 12357–12365 (2020).
55. Manikandan, V., Velmurugan, P., Park, J. H., Chang, W. S., Park, Y. J., Jayanthi, P., ... & Oh, B. T. Green synthesis of silver oxide nanoparticles and its antibacterial activity against dental pathogens. *3 Biotech* **7**, 1–9 (2017).
56. Rautela, A., & Rani, J. Green synthesis of silver nanoparticles from Tectona grandis seeds extract: characterization and mechanism of antimicrobial action on different microorganisms. *J. Anal. Sci. Technol*. **10**(1), 1–10 (2019).
57. Haq, S. et al. Fabrication of pure and moxifloxacin functionalized silver oxide nanoparticles for photocatalytic and antimicrobial activity. *J. Photochem. Photobiol B Biol.* **186**, 116–124 (2018).
58. Abel, S., Jule, L. T., Belay, F., Shanmugam, R., Dwarampudi, L. P., Nagaprasad, N., & Krishnaraj, R. Application of Titanium Dioxide Nanoparticles Synthesized by Sol-Gel Methods in Wastewater Treatment. *J. Nanomater*. **2021**(1), 3039761 (2021).
59. Hassan, Q. et al. ScienceDirect renewable energy-to-green hydrogen: a review of main resources routes, processes and evaluation. *Int. J. Hydrogen Energy*. **48**, 17383–17408 (2023).
60. Jensen, R. K. et al. Structure of the α M β 2 headpiece in the closed conformation structure of the integrin receptor α M β 2 headpiece in complex with a function-modulating nanobody. (2021).
61. Marques, F., Balcerzak, M., Winkelmann, F., Zepon, G., & Felderhoff, M. Review and outlook on highentropy alloys for hydrogen storage. *Energy Environ. Sci*. **14**(10), 5191–5227 (2021).
62. Madhavi, J. Comparison of average crystallite size by X-ray peak broadening and Williamson–Hall and size–strain plots for VO2 + doped ZnS/CdS composite nanopowder. *SN Appl. Sci.* **1**, 1–12 (2019).
63. Mani, M. et al. Studies on the spectrometric analysis of metallic silver nanoparticles (Ag NPs) using Basella alba leaf for the antibacterial activities. *Environ. Res.* **199**, 111274 (2021).
64. Mani, M. et al. Systematic green synthesis of silver oxide nanoparticles for antimicrobial activity. *Environ. Res.* **202**, 111627 (2021).
65. Mani, M. et al. A novel biogenic Allium cepa leaf mediated silver nanoparticles for antimicrobial, antioxidant, and anticancer effects on MCF-7 cell line. *Environ. Res.* **198**, 111199 (2021).
66. Stropoli, S. J., Khuu, T., Boyer, M. A., Karimova, N. V., Gavin-Hanner, C. F., Mitra, S., ... & Johnson, M. A. Electronic and mechanical anharmonicities in the vibrational spectra of the H-bonded, cryogenically cooled X−· HOCl (X= Cl, Br, I) complexes: Characterization of the strong anionic H-bond to an acidic OH group. *J. Chem. Phys*. **156**(17) (2022).
67. Windom, B. C., Sawyer, W. G., & Hahn, D. W. A Raman spectroscopic study of MoS 2 and MoO 3: applications to tribological systems. *Tribol. Lett*. **42**, 301–310 (2011).
68. Tesfaye, L. et al. Investigating Spectroscopic and Structural properties of Cr doped TiO_2 NPs synthesized through Sol gel deposition technique. *Tierärztliche Prax*. **41**, 860–872 (2021).
69. Singh, I., Mazhar, T., Shrivastava, V. & Singh Tomar, R. Bio-assisted synthesis of bi-metallic (Ag-Zn) nanoparticles by leaf extract of Azadirachta indica and its antimicrobial properties. *Int. J. Nano Dimens*. **13**, 168–178 (2022).
70. Saka, A. et al. Biological approach synthesis and characterization of iron sulfide (FeS) thin films from banana peel extract for contamination of environmental remediation. *Sci. Rep.* **12**, 1–8 (2022).
71. Nowsherwan, G. A. et al. Preparation and numerical optimization of TiO2:CdS thin films in double perovskite solar cell. *Energies* **16**, (2023).
72. Akbari, A., Mehrabian, M., Salimi, Z., Dalir, S. & Akbarpour, M. The comparison of antibacterial activities of CsPbBr3 and ZnO nanoparticles. *Int. Nano Lett.* **9**, 349–353 (2019).
73. Yang, Z. et al. Few-layer Ti3CN MXene for ultrafast photonics applications in visible band. *J. Mater.* **9**, 44–55 (2023).
74. Shiojiri, D., Iida, T., Yamaguchi, M., Hirayama, N. & Imai, Y. First-principles study of the effects of native defects on the thermoelectric properties of narrow-gap semiconducting α-SrSi2 using the hybrid functional method. *Phys. B Condens. Matter*. **634**, 413795 (2022).
75. Torad, E., Ismail, E. H., Mohamed, M. M. & Khalil, M. M. H. Tuning the redox potential of Ag@Ag2O/WO3 and Ag@Ag2S/WO3 photocatalysts toward diclofenac oxidation and nitrophenol reduction. *Mater. Res. Bull.* **137**, 111193 (2021).
76. Singh, K. et al. Corrigendum to ZnO and cobalt decorated ZnO NPs: Synthesis, photocatalysis and antimicrobial applications [Chemosphere 313 (2023) 137322] (Chemosphere 313, (S0045653522038152), (10.1016/j.chemosphere.2022.137322)). *Chemosphere* **313**, 137514 (2023).
77. Endo-Kimura, M. et al. Photocatalytic and antimicrobial properties of ag2 o/tio2 heterojunction. *ChemEngineering*. **3**, 1–18 (2019).
78. Palai, B., Sarangi, S. K. & Mohapatra, S. S. Characterization of Silver Nano-particle Coated Eichhornia crassipes fiber for Antibacterial Applications. *J. Nat. Fibers*. **19**, 1828–1836 (2022).
79. Siengchin, S., Boonyasopon, P., Sadanand, V. & Rajulu, A. V. Nanocomposite cellulose fabrics with in situ generated silver nanoparticles by bioreduction method. *J. Ind. Text.* **51**, 6258S–6275S (2022).

80. Ullah, Z. et al. Biogenic synthesis of multifunctional silver oxide nanoparticles (Ag2ONPs) using parieteria alsinaefolia delile aqueous extract and assessment of their diverse biological applications. *Microorganisms* **11**, (2023).
81. Mohanraj, R. Antimicrobial activities of metallic and metal oxide nanoparticles from plant extracts. antimicrobial nanoarchitectonics: from synthesis to applications (Elsevier Inc., (2017). https://doi.org/10.1016/B978-0-323-52733-0.00004-5
82. Muthukumar, H., Palanirajan, S. K., Shanmugam, M. K., Arivalagan, P. & Gummadi, S. N. Photocatalytic degradation of caffeine and E. Coli inactivation using silver oxide nanoparticles obtained by a facile green co-reduction method. *Clean. Technol. Environ. Policy*. **24**, 1087–1098 (2022).
83. Sun, B. et al. Insight into the effect of particle size distribution differences on the antibacterial activity of carbon dots. *J. Colloid Interface Sci.* **584**, 505–519 (2021).
84. Martínez, A. et al. Effect of essential oils on growth inhibition, biofilm formation and membrane integrity of escherichia coli and staphylococcus aureus. *Antibiotics* **10**, (2021).
85. Muhammad, S., Ali, A., Zahoor, S., Xinghua, X., Shah, J., Hamza, M., ... & Iqbal, A. Synthesis of Silver oxide nanoparticles and its antimicrobial, anticancer, anti-inflammatory, wound healing, and immunomodulatory activities-A review. *Acta Scientific Applied Physics* **3**(7), 33–48 (2023).
86. Rana, A. et al. Recent advancements in plant- and microbe-mediated synthesis of metal and metal oxide nanomaterials and their emerging Antimicrobial applications. *ACS Appl. Nano Mater.* **6**, 8106–8134 (2023).
87. Perveen, R. et al. Green versus sol-gel synthesis of ZnO nanoparticles and antimicrobial activity evaluation against panel of pathogens. *J. Mater. Res. Technol.* **9**, 7817–7827 (2020).
88. Ali, M., Ikram, M., Ijaz, M., Ul-Hamid, A., Avais, M., & Anjum, A. A. Green synthesis and evaluation of ntype ZnO nanoparticles doped with plant extract for use as alternative antibacterials. *Appl. Nanosci.* **10**, 3787–3803 (2020).
89. Sengul, A. B. & Asmatulu, E. Toxicity of metal and metal oxide nanoparticles: a review. *Environ. Chem. Lett.* **18**, 1659–1683 (2020).
90. Siddiqui, V. U., Ansari, A., Chauhan, R. & Siddiqi, W. A. Green synthesis of copper oxide (CuO) nanoparticles by Punica granatum peel extract. *Mater. Today Proc.* **36**, 751–755 (2019).
91. Abbas, S. F., Haider, A. J., Al-Musawi, S. & Selman, M. K. Antibacterial Effect of Copper Oxide nanoparticles prepared by Laser Production in Water against Staphylococcus aureus and Escherichia coli. *Plasmonics*. https://doi.org/10.1007/s11468-023-02135-x (2023).
92. Abou-Dobara, M. I., Kamel, M. A., El-Sayed, A. K. A. & El-Zahed, M. M. Antibacterial activity of extracellular biosynthesized iron oxide nanoparticles against locally isolated β-lactamase-producing Escherichia coli from Egypt. *Discov. Appl. Sci.* **6**, (2024).
93. Ouerghi, O. et al. Journal Pre of. *J. Drug Deliv. Sci. Technol.* **102581.** https://doi.org/10.1016/j.jddst.2021.102581 (2021).
94. Wong, C. W. et al. Response surface methodology optimization of mono-dispersed MgO nanoparticles fabricated by Ultrasonic-assisted Sol–Gel Method for Outstanding Antimicrobial and Antibiofilm activities. *J. Clust Sci.* **31**, 367–389 (2020).
95. Rheima, A. M., Anber, A. A., Shakir, A. A., Hameed, A. S. & Hameed, S. A. Novel method to synthesis nickel oxide nanoparticles for antibacterial activity. *Iran. J. Phys. Res.* **20**, 51–55 (2020).
96. Rahmat, M. et al. Bionanocomposite of au decorated MnO2 via in situ green synthesis route and antimicrobial activity evaluation. *Arab. J. Chem.* **14**, 103415 (2021).
97. Kumar, S., Ahmed, F., Shaalan, N. M. & Saber, O. Biosynthesis of ceo2 nanoparticles using egg white and their antibacterial and antibiofilm properties on clinical isolates. *Crystals*. **11**, 1–12 (2021).
98. Li, D. et al. The interaction of Ag2O nanoparticles with Escherichia coli: inhibition–sterilization process. *Sci. Rep.* **11**, 1–9 (2021).

Acknowledgements

Our sincere gratitude goes to the Indian Institute of Technology, Department of Material Science and Metallurgical Engineering (Combinatorial Laboratory), and Dambi Dollo University for their support in the laboratory work conducted for this article. Additionally, we would like to express our appreciation to the Joint Ph.D. Program of The Ministry of Education Ethiopia and the Ministry of Innovation and Technology for providing Dambi Dollo University with the opportunity to engage in a joint Ph.D. supervision program with IIT, Hyderabad.

Author contributions

Conceptualization, A, S, SR. D, R. K, R. D, N. M and N. N.; Data curation, A, S, SR. D, R. K, R. D, N. M and N. N.; Analysis and Validation, A, S, SR. D, LT. J, R. K, R. D, N. M and N. N.; Formal analysis, A, S, SR. D, LT. J, R. K, R. D, N. M and N. N; Investigation, A, S, SR. D, R. K, R. D, N. M and N. N.; Methodology, A, S, SR. D, R. K, R. D, N. M and N. N.; Project administration, K.R and SR. D. Resources, A, S, SR. D, R. K, R. D, N. M and N. N.; Software, A, S, SR. D, R. K, R. D, N. M and N. N., Supervision, K. R. and SR. D; Validation, A, S, SR. D, R. K, R. D, N. M and N. N.; Visualization, A, S, SR. D, R. K, R. D, N. M and N. N.; Writing—original draft, A, S, SR. D, R. K, R. D, N. M and N. N., Data Visualization, Editing and Rewriting, A, S, SR. D, LT. J, R. K, R. D, N. M and N. N.

Declarations

Competing interests

The authors declare no competing interests.

Additional information

Correspondence and requests for materials should be addressed to R.K.

Reprints and permissions information is available at www.nature.com/reprints.

Publisher's note Springer Nature remains neutral with regard to jurisdictional claims in published maps and institutional affiliations.